



## Accepted Article

**Title:** The Role of Surface Termination in Halide Perovskite for Efficient Photocatalytic Synthesis

**Authors:** Qi Chen, Yuanyuan Dong, Kailin Li, Wenjia Luo, Cheng Zhu, Haoliang Guan, Hao Wang, Lanning Wang, Kailin Deng, Huanping Zhou, Haipeng Xie, Yang Bai, and Yujing Li

This manuscript has been accepted after peer review and appears as an Accepted Article online prior to editing, proofing, and formal publication of the final Version of Record (VoR). This work is currently citable by using the Digital Object Identifier (DOI) given below. The VoR will be published online in Early View as soon as possible and may be different to this Accepted Article as a result of editing. Readers should obtain the VoR from the journal website shown below when it is published to ensure accuracy of information. The authors are responsible for the content of this Accepted Article.

**To be cited as:** *Angew. Chem. Int. Ed.* 10.1002/anie.202002939

**Link to VoR:** <https://doi.org/10.1002/anie.202002939>

## RESEARCH ARTICLE

# The Role of Surface Termination in Halide Perovskite for Efficient Photocatalytic Synthesis

Yuanyuan Dong,<sup>[a]</sup> Kailin Li,<sup>[a]</sup> Wenjia Luo,<sup>[b]</sup> Cheng Zhu,<sup>[a]</sup> Haoliang Guan,<sup>[a]</sup> Hao Wang,<sup>[a]</sup> Lanning Wang,<sup>[a]</sup> Kailin Deng,<sup>[c]</sup> Huanping Zhou,<sup>[d]</sup> Haipeng Xie,<sup>[e]</sup> Yang Bai,<sup>[a]</sup> Yujing Li\*<sup>[a]</sup> and Qi Chen\*<sup>[a]</sup>

[a] Dr Y. Dong, K. Li, Ch. Zhu, H. Guan, H. Wang, L. Wang, Dr Y. Bai, Prof. Y. Li and Prof. Q. Chen. Experimental Center of Advanced Materials, Beijing Key Laboratory of Nanophotonics and Ultrafine Optoelectronic Systems, School of Materials Science and Engineering, Beijing Institute of Technology, Beijing 100081, P.R. China.

E-mail: [qic@bit.edu.cn](mailto:qic@bit.edu.cn), [yili@bit.edu.cn](mailto:yili@bit.edu.cn)

[b] Prof. W. Luo, School of Chemistry and Chemical Engineering, Southwest Petroleum University, Chengdu, 610500, P.R. China.

[c] Dr K. Deng, Key Laboratory of Agro-products Quality and Safety Control in Storage and Transport Process, Ministry of Agriculture and Rural Affairs/Institute of Food Science and Technology, Chinese Academy of Agricultural Sciences, Beijing 100193, P.R. China.

[d] Prof. H. Zhou, Department of Materials Science and Engineering, College of Engineering, Peking University, Beijing 100871, P. R. China

[e] Prof. H. Xie, School of Physics and Electronics, Central South University, Changsha, Hunan 410083, P.R. China.

Supporting information for this article is given via a link at the end of the document. ((Please delete this text if not appropriate))

**Abstract:** Halide perovskites have received extensive attention in the field of photocatalysis owing to their excellent optoelectronic properties. However, the semiconductor properties of halide perovskite surface and the influences on the photocatalytic performances have not been systematically clarified. Here we employ the conversion of triose (e.g. 1,3-dihydroxyacetone (DHA)) as a model reaction to explore the surface termination of MAPbI<sub>3</sub>. By rational design of the surface termination for MAPbI<sub>3</sub>, we substantially improve the production rate of butyl lactate to 7719 µg/g cat./h under visible light illumination. It reveals that MAI-terminated MAPbI<sub>3</sub> surface governs the photocatalytic performance. Specially, MAI-terminated surface is susceptible to iodide oxidation, which thus promotes the exposure of Pb(II) as active sites for this photocatalysis process. Moreover, MAI-termination induces p-doping effect near the surface for MAPbI<sub>3</sub>, which facilitates the carrier transport and thus photosynthesis. The understanding of the surface termination in MAPbI<sub>3</sub> photocatalyst suggests a new avenue to engineer halide perovskite semiconductor materials for future photocatalysis.

## Introduction

The hybrid ABX<sub>3</sub> perovskite semiconductors have revolutionized photovoltaics, enabling solution-processable solar cells to reach the power conversion efficiency of 25.2%.<sup>[1]</sup> They have also been demonstrated to show good performance in high-gain photodetectors,<sup>[2]</sup> light-emitting diodes,<sup>[3]</sup> and lasers.<sup>[4]</sup> The excellent optoelectronic properties are attributed to strong light absorption, long charge-carrier lifetimes and diffusion lengths.<sup>[5]</sup> Given the above beneficial optoelectronic properties, the halide perovskite materials have also received extensive attention in the field of photocatalysis.<sup>[6]</sup> Under visible light irradiation, halide perovskite photocatalysts could catalyze the dye degradation,<sup>[7]</sup> water splitting,<sup>[6f]</sup> the reduction of CO<sub>2</sub>,<sup>[6a]</sup> and the oxidation of benzylic alcohols.<sup>[8]</sup> To achieve good separation/migration of photoexcited holes and electrons, many composite/heterojunction photocatalytic semiconductors have been developed. MAPbI<sub>3</sub>/rGO, CsPbBr<sub>3</sub> NC/BZNM/RGO, α-Fe<sub>2</sub>O<sub>3</sub>/Amine-RGO/CsPbBr<sub>3</sub>, CPB-PCN, CsPbBr<sub>3</sub>/Cs<sub>4</sub>PbBr<sub>6</sub> and FAPbBr<sub>3</sub>/TiO<sub>2</sub> hybrid photocatalyst are prepared and exhibit the improved photocatalytic performance.<sup>[6c, 9]</sup> Recently, Yan et al. discover that

the APbBr<sub>3</sub> (A = Cs or MA) type perovskite colloids can selectively catalyze the formation of C-C bond via a new mode of small molecule activation.<sup>[6e]</sup> The as-prepared perovskite photocatalysts NCs are effective with a TON of over 52,000 for α-alkylation, 3 orders of magnitude higher than conventional Ir- or Ru-based catalysts. Moreover, the perovskite photocatalysts are much more economical than conventional organometallic compound (2-order cost lower). The efficient photocatalytic performances and low-cost render halide perovskite as new promising candidates for broad application in photocatalytic chemical synthesis.

In the aspect of photocatalysis, controlling the semiconducting properties of photocatalysts is the primary concern, because they determine how much photoexcitation occurs in a semiconductor under solar illumination and how many photoexcited carriers reach the surface where the photocatalytic reaction takes place.<sup>[10]</sup> Given a specific semiconductor material, surface modifications are important not only to activate the semiconductor but also to facilitate charge separation under photoexcitation in photocatalytic process. It is reported that the electronic conductivity of bulk MAPbI<sub>3</sub> can be tuned between p-type and n-type by controlling growth conditions.<sup>[11]</sup> However, the semiconductor properties of the halide perovskite materials surface have not been systematically reported, especially in the field of photocatalysis. Specially, MAPbI<sub>3</sub> has two major surface termination (MAI and PbI<sub>2</sub>).<sup>[12]</sup> MAI-terminated surface are easily prone to expose the Pb(II) sites caused by the oxidation of iodide, while the PbI<sub>2</sub>-terminated surface are relative robust.<sup>[13]</sup> The difference in surface termination of MAPbI<sub>3</sub> will affect the activation of reactant molecules and the carrier migration in the photocatalytic process to some extent. Therefore, it is highly desirable to study the termination, clarify the surface species and the surface semiconductor properties of MAPbI<sub>3</sub> perovskite.

Herein, we employ the conversion of triose (e.g. DHA) as a model reaction, commonly using Pb(II) as a catalyst,<sup>[14]</sup> to explore the surface termination of MAPbI<sub>3</sub>, and further investigate its effects on photocatalytic performance. MAPbI<sub>3</sub> photocatalysts are readily prepared via the coevaporation method under the certain relative humidity in the customized glove box (Figure 1a and Scheme S1). The photocatalytic synthesis reaction of butyl lactate from DHA and butanol is shown in Figure 1b. We demonstrate the yield of butyl lactate is 77 mg/L over MAPbI<sub>3</sub> photocatalyst.

## RESEARCH ARTICLE

According to our investigation, this is the first report of photocatalytic synthesis of butyl lactate from triose under visible light illumination at room temperature. A series of characterizations indicate that the desirable MAI-terminated MAPbI<sub>3</sub> perovskite surface facilitates the effective photocatalytic synthesis of butyl lactate. MAI-terminated surface are easily prone to expose the Pb(II) sites caused by the oxidation of iodide, which are considered as the active sites for this photocatalytic synthesis. Furthermore, MAI-terminated induces p-doping effect near the surface for MAPbI<sub>3</sub>. A photocatalytic mechanism is hence proposed. Upon solar light illumination, electrons and holes are generated in MAPbI<sub>3</sub>. The photo-generated holes are consumed to oxidize DHA into pyruvaldehyde, whereas the exposed Pb(II) sites on MAI-terminated MAPbI<sub>3</sub> surface contribute to promote the pyruvaldehyde and butanol substrates towards the final product.

## Results and Discussion

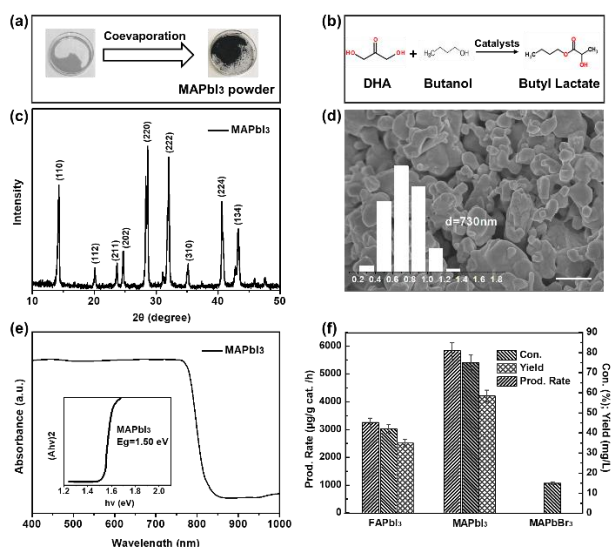


**Figure 1.** (a) Scheme of the preparation of MAPbI<sub>3</sub> via co-evaporation method. (b) The schematic diagram of the conversion of DHA and butanol into butyl lactate over catalyst. (c) XRD pattern. (d) SEM image and (e) UV-vis absorption spectra of MAPbI<sub>3</sub>. (f) The photocatalytic activities of MAPbI<sub>3</sub>, FAPbI<sub>3</sub> and MAPbBr<sub>3</sub> photocatalysts.

MAPbI<sub>3</sub> powder is prepared using a simple co-evaporation method with the customized glove box (Scheme S1) under a relative humidity of 35%±5% (Figure 1a), with further procedural details described in the Experimental Section. The powder X-ray diffraction (XRD) patterns (Figure 1c) verify the tetragonal phase of MAPbI<sub>3</sub>.<sup>[15]</sup> The scanning electron microscopy (SEM) image (Figure 1d) shows that the average size of MAPbI<sub>3</sub> is around 730 nm. The optical absorption edge of MAPbI<sub>3</sub> is determined from UV-Vis absorption spectrum (Figure 1e) with the typical band gap of 1.50 eV (827 nm).<sup>[6]</sup> With the verified structure, MAPbI<sub>3</sub> is thus employed to photocatalyze the reaction between DHA and butanol as described in Figure 1b. The photocatalytic synthesis of butyl lactate is conducted in a side-irradiation sealed quartz vessel with a Xe-lamp (CEL-S500) and a 420 nm cut-off filter. The product is analyzed by gas chromatograph-mass spectrometer

(GCMS) and confirms the formation of target product butyl lactate (Figure S1). Figure 1f shows that MAPbI<sub>3</sub> exhibits good photocatalytic performances with the production rate of 5837 µg/g cat./h and the yield of 58.4 mg/L, respectively. Other perovskite materials have also been tested for this reaction (Figure 1f and Table S1). It can be seen that MAPbI<sub>3</sub> and FAPbI<sub>3</sub> could effectively convert DHA into butyl lactate. Although the conversion of DHA reaches 15%, the Br-based perovskite materials are inactive for the synthesis of butyl lactate. It implies that some other products are produced in this photocatalytic process (Figure S1). Moreover, the MAPbBr<sub>1-x</sub> (x=Br/I molar ratio) could promote the photocatalytic synthesis of butyl lactate (Figure S2). The yield of butyl lactate is positively related with the amount of I.

Given the reported work on the conversion of triose catalyzed by Pb(II) ions at the relative high temperature<sup>[14]</sup>, it is supposed that the naked Pb(II) sites on the surface of MAPbI<sub>3</sub> play a crucial role in this photocatalytic reaction. Due to the chemical instability, MAPbI<sub>3</sub> will decompose to HI, CH<sub>3</sub>NH<sub>2</sub> and PbI<sub>2</sub>, etc. in polar solvent.<sup>[16]</sup> PbI<sub>2</sub> is confirmed to be inactive towards this photocatalytic reaction (Table S2). Additionally, the amount of Pb dissolved in the reaction supernatant is only 7.8 µg/mL (determined by ICP) and hence can be considered to be negligible compared with the amount of MAPbI<sub>3</sub> catalyst (3.3 mg/mL in terms of Pb). We further conduct a contrast experiment (Table S2) to exclude the possible influence of the leaking Pb(II) ions. The oleophilic TiO<sub>2</sub> is added into the reactant solution with free Pb(II) ions and irradiated under the same condition. No butyl lactate can be detected. Therefore, we reason that the leaking Pb(II) ions in solution are inactive. The naked Pb(II) sites in inorganic-framework on the surface of MAPbI<sub>3</sub> are considered as the catalytic sites for the photocatalytic synthesis of butyl lactate. Owing to the lower oxidation potential, iodide is easily oxidized to form iodide vacancies, leading to the exposed Pb(II) species on the surface of MAPbI<sub>3</sub>.<sup>[13b]</sup> To confirm this speculation, it is important to understand the surface termination of MAPbI<sub>3</sub>. In view of the crystal structure of this ionic compound, there are two major termination: 1) MA<sup>+</sup> cations hydrogen bonded with inorganic scaffold, and 2) partially covalent I<sup>-</sup> in PbI<sub>4</sub><sup>2-</sup> octahedron. Unfortunately, these two species are most likely catalytically inert based on control experiment (Table S2). Considering the difference in ionic radius between halogen ions and the formation energy of halide perovskites<sup>[17]</sup>, the surface defects may be responsible for the different photocatalytic results of halide perovskites (Figure 1f and Figure S2). It is reported that the formation energy of iodine vacancies (V<sub>I</sub>) is low, which favors the formation of defects and the corresponding naked Pb(II) sites, especially at the surface.<sup>[13a]</sup> We hence propose that the positively charged Pb resulting from the iodine vacancies/defects, serving as the central sites, are responsible for the catalytic process.

To identify the role of Pb, methimazole (MMI) is selected to passivate the exposed Pb(II) sites based on the Lewis acid-base theory (Figure 2a),<sup>[18]</sup> wherein the PbI<sub>2</sub>-MMI/MAI-PbI<sub>2</sub>-MMI adduct is formed via the Pb-S coordination reaction. The diffraction peak of 9.85° in XRD patterns (Figure 2b) confirms the formation of the adduct, which is consistent with our previous work.<sup>[18a]</sup> The Fourier-transform infrared spectra (FTIR) in Figure 2c also provide detailed evidence about the successful passivation. The fingerprint peaks associated to the S=C stretching for pristine MMI at 738 cm<sup>-1</sup> shifts to 735 cm<sup>-1</sup> after MAPbI<sub>3</sub> treated with MMI (denoted as MAPbI<sub>3</sub>-S). The down-shift of the S=C vibration in MMI is indicative of the interaction between Pb and S, leading to

## RESEARCH ARTICLE

the weakened S=C bond strength. The electronic states of Pb and S determined by X-ray photoelectron spectroscopy (XPS) further confirm the interaction between Pb and S. As Figure 2d shows, the peak at 138.1 eV is assigned to the Pb 4f 7/2 of MAPbI<sub>3</sub>. After treatment with MMI, the existence of S at the surface is evidenced by the observed apparent signals of S 2p. Furthermore, the Pb 4f peak of MAPbI<sub>3</sub>-S significantly shifts to the higher binding energy. It thus verifies that the exposed Pb(II) sites are successfully passivated by MMI molecule at the perovskite surface via the Pb-S coordination.

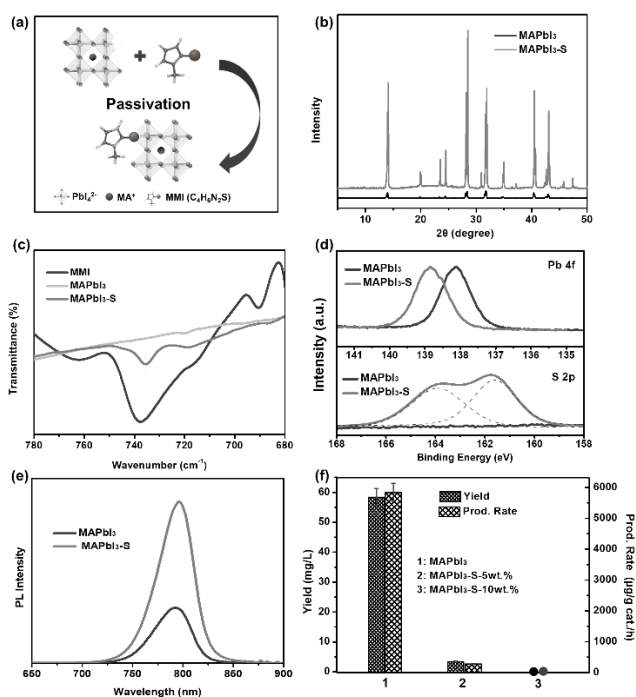


**Figure 2.** (a) The schematic diagram of the passivation of MAPbI<sub>3</sub>. (b) XRD patterns of original and MAPbI<sub>3</sub>-S photocatalysts. (c) FTIR spectra of MMI, original and passivated MAPbI<sub>3</sub>. (d) The Pb 4f and S 2p signal of MAPbI<sub>3</sub> and MAPbI<sub>3</sub>-S. (e) Steady-state PL spectra and (f) photocatalytic activities of MAPbI<sub>3</sub> and MAPbI<sub>3</sub>-S photocatalysts.

Upon the effective passivation, the exposed Pb(II) sites are covered by MMI, which implies that the iodine vacancies in MAPbI<sub>3</sub> are efficiently repaired. The crystal structure with fewer defects is evidenced by the increased intensity of XRD diffraction peak of MAPbI<sub>3</sub>-S sample (Figure 2b). Photoluminescence (PL) spectra further verifies the well-passivated surface of MAPbI<sub>3</sub>-S (Figure 2e). Compared with MAPbI<sub>3</sub> reference, the PL intensity of MAPbI<sub>3</sub>-S significantly enhanced, which further confirms the defects are effectively healed. Namely, the exposed Pb(II) sites at the MAPbI<sub>3</sub> surface are well poisoned by MMI. The photocatalytic activities of MAPbI<sub>3</sub>-S should decrease because of the sheltered Pb(II) sites. As Figure 2f shows, after treatment with 5wt.% MMI, the yield declines to only 10% of the untreated one. By further increasing the amount of poisoning species to 10 wt.%, the target product butyl lactate cannot be detected. The results serve as solid evidences that the naked Pb(II) sites on MAPbI<sub>3</sub> surface play an essential role in this reaction. Moreover, the control experiments (Table S2) are carried out under the same reaction conditions. Neither PbI<sub>2</sub>, MAI and the leaking Pb(II) ions can

catalyze the reaction alone. Additionally, Table S2 shows that the reaction cannot proceed with solely the visible light or the MAPbI<sub>3</sub> at dark. Based on the above investigation, it is found that the MAPbI<sub>3</sub> with the exposed Pb(II) sites could effectively convert DHA and butanol into butyl lactate at room temperature with visible light.

Although the naked Pb(II) site has been confirmed as a terminal species, it is the result of the iodide vacancies resulting from the oxidation of surface iodine. In view of the two major termination structure (MAI or PbI<sub>2</sub>), it is still necessary to further explore the surface termination of MAPbI<sub>3</sub>. The preparation process (details in SI) hence be investigated in detail because the surface of MAPbI<sub>3</sub> will restructure during the moisture annealing process.<sup>[19]</sup> In a moisture annealing process, highly hygroscopic MA cations pull moisture from the environment. Water molecules adsorb on the surface vacancies or edges/boundaries, leading to the surface solvation/dissolution of perovskite crystals, and then facilitate the merging of initial primary crystals into larger grains.<sup>[20]</sup> SEM images of MAPbI<sub>3</sub>-x (Figure S3) agree with the above reported phenomenon. Therefore, the ambient humidity is an important factor affecting the surface reconstruction. We thus prepare a series of MAPbI<sub>3</sub>-x materials via moisture annealing technique in the customized glove box (Scheme S1), where x represents the relative humidity of 15%, 25%, 35%, 45% and 55% with the fluctuation within 5%.

**Table 1.** The surface composition of moisture-annealed MAPbI<sub>3</sub> determined by XPS.

Catalyst	Pb	I	N	I/Pb	N/Pb
MAPbI <sub>3</sub> -15%	17.69%	52.6%	9.69%	2.97	0.55
MAPbI <sub>3</sub> -25%	17.07%	53.07%	9.72%	3.11	0.57
MAPbI <sub>3</sub> -35%	15.43%	53.27%	10.38%	3.45	0.67
MAPbI <sub>3</sub> -45%	16.02%	54.58%	9.83%	3.41	0.61
MAPbI <sub>3</sub> -55%	16.33%	55.36%	9.64%	3.39	0.59

The surface composition is determined by XPS in Figure 3a and Table 1. Under the lower relative humidity ( $\leq 35\% \pm 5\%$ ), the amount of I and N gradually increase with the humidity, while the amount of Pb decreases. According to the moisture annealing process, the hydrophilic MA cations pull moisture from the environment, facilitating the diffusion of MA cations.<sup>[21]</sup> Therefore, it is deduced that the MAI gradually enriches on the surface with the increasing humidity, and reaches a maximum at the humidity of 35%. Namely, MAPbI<sub>3</sub> surface is terminated by MAI under the lower humidity ( $\leq 35\% \pm 5\%$ ), resulting in a more p-type feature on the surface. When the humidity further increases, the amount of N decreases on the MAPbI<sub>3</sub>-x surface, accompanied with the increment of the Pb amount (Table 1). It implies that MAPbI<sub>3</sub> surface is terminated by PbI<sub>2</sub> under the relative high humidity ( $>35\% \pm 5\%$ ), leading to a more n-type feature on the surface. These observations can be attributed to the self-doping effects during the moisture annealing process.<sup>[22]</sup>

## RESEARCH ARTICLE

The self-doping effects are further confirmed by the valence band spectra in Figure 3b. Under the low relative humidity ( $\leq 35\% \pm 5\%$ ), the Fermi level of MAPbI<sub>3</sub> moves from 1.27 to 0.31 eV from the valence band maximum (VBM) with the increase of humidity. Given the band gap of 1.5 eV (Figure 1e) for the perovskite, the shift puts the Fermi level very close to the VBM. It suggests that the surface of MAPbI<sub>3</sub> tends to be a more p-type feature. At the high humidity ( $>35\% \pm 5\%$ ), the Fermi level from VBM increases from 0.31 to 1.29 eV, which implies that Fermi level moves close to the conduction band minimum (CBM). The surface of MAPbI<sub>3</sub> tends to be a more n-type feature at this point.

Furthermore, we have employed density functional theory (DFT) to clarify the band structure of the as-designed MAPbI<sub>3</sub>. The details about computation methods and structure models are described in the SI. Figure 3c and Figure S4 show the band structure of MAI-terminated and PbI<sub>2</sub>-terminated MAPbI<sub>3</sub>, respectively. The band structure is significantly different between them. After the vacuum energy level alignment, the schematic diagram of the two energy band structures is described in Figure 3d. Compared with PbI<sub>2</sub>-terminated MAPbI<sub>3</sub>, the VBM of MAI-terminated MAPbI<sub>3</sub> slightly shifts up and is closer to the vacuum energy level. It suggests that MAI-terminated MAPbI<sub>3</sub> tends to be a more p-type feature on the surface, which is consistent with our experimental results.

The photocatalytic performances of the MAPbI<sub>3</sub>-x materials are shown in Figure 3a. Clearly, the yield of butyl lactate depends on the humidity, reaching the maximum of 58.4 mg/L with the humidity of 35%. The production rate of target product also follows the similar trend (Figure S5). Combined with the changes of the surface N amount with humidity, it is inferred that the photocatalytic activities could be improved with the enrichment of MAI on MAPbI<sub>3</sub> surface. Namely, MAI-terminated surface could facilitate the photocatalytic reaction. This should be attributed to the fact that the iodine species on the MAI-terminated surface are easily oxidized, leading to the exposed Pb(II) as the terminating species in MAPbI<sub>3</sub>.<sup>[13b, 23]</sup> Whereas, the augmentation of PbI<sub>2</sub> on the MAPbI<sub>3</sub> surface would decrease the photocatalytic activities. Because the PbI<sub>2</sub>-terminated surface is robust owing to the stronger (shorter) Pb-I bonds, it is not easy to form iodide vacancies and the resulting naked Pb(II) sites.<sup>[12]</sup> DFT is further employed to calculate the formation energies of iodine vacancies between MAI-terminated and PbI<sub>2</sub>-terminated MAPbI<sub>3</sub>. The top view of the MAI- and PbI<sub>2</sub>-terminated MAPbI<sub>3</sub> (110) surfaces without and with iodine vacancy is shown in Figure S6. The calculation suggests that the formation energy of iodine defects is slightly higher on PbI<sub>2</sub>-terminated ( $\Delta G=1.80$  eV) than on MAI-terminated ( $\Delta G=1.74$  eV) MAPbI<sub>3</sub>, which is consistent with the experimental results.

Additionally, the surface reconstruction, stemming from the destruction and reconstruction of the bond between MA<sup>+</sup> and the Pb-I octahedron,<sup>[24]</sup> leads to the crystal lattice distortion and the corresponding microstrain.<sup>[20b]</sup> The resulted microstrain can mainly be decerned in the FWHM of XRD diffraction peaks of MAPbI<sub>3</sub>-x (Figure S7). Figure S8 shows the calculated microstrain of MAPbI<sub>3</sub>-x based on the modified Williamson-Hall (W-H) method (Eq. S1).<sup>[25]</sup> It is found that the microstrain of MAPbI<sub>3</sub>-x basically displays a "volcano-shaped" dependence with the humidity. The microstrain resulting from the surface reconstruction possibly induce the formation of defects including the surface and bulk defects. The carrier lifetime determined by the TRPL (Figure S9) can distinguish these defects to some extent. We fit the decay

curves by the biexponential equation:  $Y=A_1 \exp(-t/\tau_1)+A_2 \exp(-t/\tau_2)$ , where the short lifetime  $\tau_1$  stands for the surface nonradiative recombination and the long lifetime  $\tau_2$  for the bulk recombination. As the humidity increases, the surface nonradiative recombination lifetime  $\tau_1$  displays the similar trend to that of microstrain (Table S3). It is deduced that the microstrain stemming from the reconstruction could lead to the formation of surface defects (e.g. V<sub>I</sub>), resulting in the exposure of Pb(II) sites. The trend of the photocatalytic activity described in Figure S10 further proves it. However, MAPbI<sub>3</sub>-15% seems to be an exception, which may originate from the excessive defects caused by an extreme microstrain.

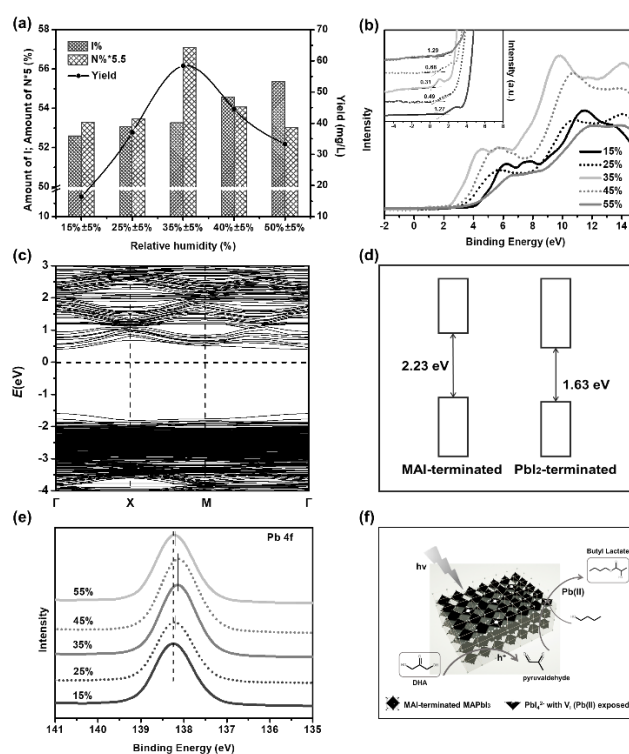


**Figure 3.** (a) The relationship plots among the amount of N and I determined by XPS, the yield of butyl lactate and the relative humidity. (b) The valence band spectra of the MAPbI<sub>3</sub>-x materials. (c) Band structure of MAI-terminated MAPbI<sub>3</sub> with iodine vacancies. (d) The schematic diagram of the energy band structure of MAI-terminated and PbI<sub>2</sub>-terminated MAPbI<sub>3</sub> upon the vacuum energy level alignment. (e) High resolution Pb 4f XPS spectra of the MAPbI<sub>3</sub>-x materials. (f) The schematic diagram of the photocatalytic mechanism for the synthesis of butyl lactate over MAPbI<sub>3</sub>.

Furthermore, the destruction and reconstruction of the bond between MA<sup>+</sup> and the Pb-I octahedron would also lead to changes in the electronic properties of elements.<sup>[26]</sup> Specifically, the binding energy of Pb 4f first shifts to lower binding energy and then shifts to higher binding energy (Figure 3e). Not only for Pb, the shifts of the binding energy of other elements show the similar trend (Figure S11). According to the previous results, the shift to low binding energy indicating the elongated bond of Pb-I, which suggests that the Fermi energy level moves downward in terms of band structure.<sup>[27]</sup> It suggests the surface of semiconductor tends to be a more p-type feature, which is consistent with the results of valence band spectra (Figure 3b). On the contrary, the shift to high binding energy indicates a more n-type nature of the

## RESEARCH ARTICLE

surface. The influences of surface self-doping on the photocatalytic activities are described in Figure S12. With the addition of hole scavenger, the production rate of target product drops to 4%, which verifies the crucial role of photo-generated hole in this photocatalysis system.

Based on the above analyses, it can be inferred that MAI-terminated MAPbI<sub>3</sub> could facilitate the photocatalytic synthesis of butyl lactate. Thereinto, MAI-terminated surface induces the p-type self-doping of MAPbI<sub>3</sub>, which promote the oxidation of DHA to pyruvaldehyde.<sup>[28]</sup> The GC spectrum of Figure S13 confirms the pyruvaldehyde in the reaction product. Moreover, the pyruvaldehyde further reacts with butanol to produce butyl lactate via the path of K-E (consecutive keto–enol tautomerization) or 1,2-H (1,2-hydride shift), where the exposed Pb(II) on MAI-terminated MAPbI<sub>3</sub> surface decreases the activation barrier.<sup>[14, 29]</sup> Hereby, we propose a photocatalytic mechanism as illustrated in Figure 3f. Upon the visible light illumination, electrons and holes are generated in MAPbI<sub>3</sub>. The photogenerated holes are consumed to oxidize the reactant DHA into pyruvaldehyde (Figure S13), whereas the photogenerated electrons are utilized by the exposed Pb(II) to promote the pyruvaldehyde and butanol substrates to produce the final product butyl lactate.

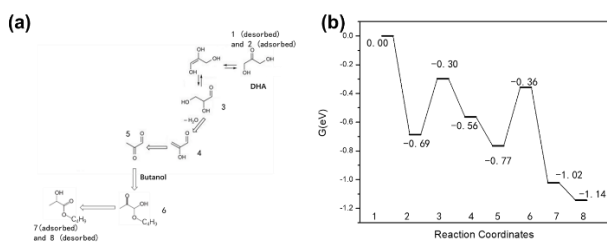


**Figure 4.** (a) Proposed reaction mechanism based on reference 14 for the conversion of DHA to butyl lactate. (b) Free energy diagram for the conversion of DHA into butyl lactate over MAI-terminated MAPbI<sub>3</sub> photocatalyst with iodine vacancies under irradiated condition.

To further confirm the crucial role of the exposed Pb(II) sites caused by the iodine vacancies, we simulate the adsorption of reactants, intermediate and products on the surface of MAI-terminated MAPbI<sub>3</sub> photocatalyst with and without iodine vacancies based on this reaction mechanism (Figure 4a). Top and side view of the slab for MAI-terminated MAPbI<sub>3</sub> with and without iodine vacancy are shown in S14. The geometries of the adsorbed intermediates are listed in Table S4. The crucial role of the exposed Pb(II) sites caused by the iodine vacancy is obvious. When an iodine vacancy is present, one of the octahedrons on the surface is missing a corner and the adjacent Pb site is exposed. As an adsorbate molecule approaches the surface, one oxygen atom from the adsorbate bonds with the exposed Pb atom (Top and side view of state 2 in the first two columns of Table S4). The resulting adsorption free energy of DHA ( $\Delta G_{1-2}$ ) is -0.69 eV (Figure 4b), which implies that DHA can spontaneously adsorb on the surface of MAPbI<sub>3</sub> photocatalyst with iodine vacancies. The activation of DHA and subsequent reaction can be continued. However, the cleans surface of MAPbI<sub>3</sub> without iodine vacancies is chemically saturated, which attracts the adsorbates mainly through dispersion effects (Top and side view of state 2 in the last two columns of Table S4), leading to weak adsorption and difficulty in the activation of reactant. The resulting adsorption free energy of DHA ( $\Delta G_{1-2}$ ) is 0.02 eV (Figure S15), which implies that

DHA requires additional energy to adsorb on the surface of MAPbI<sub>3</sub> photocatalyst without iodine vacancies. Obviously, the exposure of Pb(II) sites is very important for the adsorption and activation of DHA on MAPbI<sub>3</sub> photocatalyst, whereas it is the first prerequisite step of the reaction.

To further improve the photocatalytic activities, it is an effective strategy to expose more Pb(II) sites on the surface of MAPbI<sub>3</sub> as previously mentioned. It has been reported that iodide is easy to be oxidized even in ambient processing due to its low oxidation potential.<sup>[13b]</sup> We thus conducted ageing process to create more surface defects or vacancies (e.g.  $V_I$ ,  $V_{MA}$ ) to regulate the exposure of Pb(II) sites. The aged sample is designated as MAPbI<sub>3</sub>-A1 and MAPbI<sub>3</sub>-A2 with the different ageing time (Experiment section in supporting information). The fresh MAPbI<sub>3</sub> and aged counterpart show the similar XRD patterns (Figure 5a), indicating that the crystal structure of MAPbI<sub>3</sub> did not change significantly. However, the full width at half maximum (FWHM) of the (220) crystal plane gradually increases from 0.147 to 0.164, which may result from the microstrain between perovskite crystals during ageing. The broadening of the strongest peak suggests a reduced crystallinity of the materials.<sup>[30]</sup> It implies that the surface defects of MAPbI<sub>3</sub> may increase after ageing. Figure 5b depicts the steady-state PL spectra of the fresh and aged MAPbI<sub>3</sub>. The decreased PL intensity indicate the enhanced non-radiative recombination, which results from the augmented surface defects of the aged sample (MAPbI<sub>3</sub>-A1 and MAPbI<sub>3</sub>-A2). The broadening of the emission spectra of the aged samples comes from the hydration and/or hydrogen bonding interactions between water molecules, organic cation ( $MA^+$ ) and halide ions,<sup>[31]</sup> leading to the formation of new surface defects. A blue shift of 16 nm for PL peak of MAPbI<sub>3</sub>-A1 also suggests the formation of additional defects after ageing.<sup>[32]</sup>

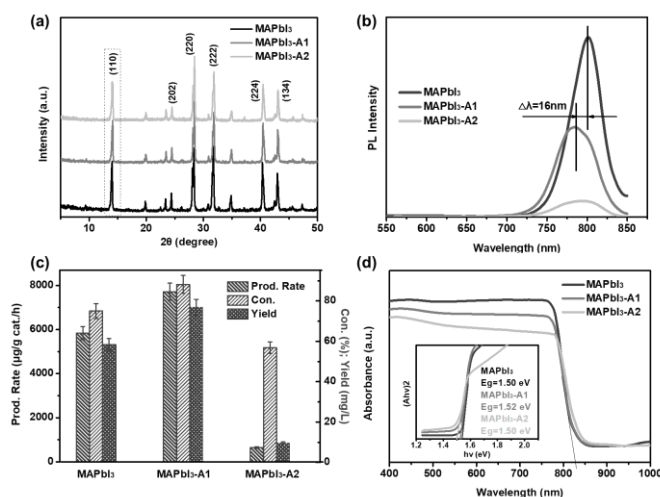


**Figure 5.** (a) XRD patterns, (b) steady-state PL spectra, (c) the photocatalytic activities and (d) UV-vis absorption spectra of fresh and aged MAPbI<sub>3</sub>.

The fresh and aged MAPbI<sub>3</sub> are hence evaluated for the photocatalytic tests (Figure 5c). Compared with MAPbI<sub>3</sub>, the aged sample MAPbI<sub>3</sub>-A1 exhibits an enhanced performance in conversion, yield and production rate of butyl lactate from triose. According to the abovementioned investigations, the improved photocatalytic activities should be attributed to the more exposed Pb(II) sites caused by the augmented surface defects. However,

## RESEARCH ARTICLE

the photocatalytic activities of MAPbI<sub>3</sub>-A2 obviously decreases (Figure 5c). The significantly reduced PL and XRD peak intensity (Figure 5a and 5b) indicates the further augmented defects of MAPbI<sub>3</sub>-A2. Namely, the excessive ageing induces too much surface defects and hence decreases the photocatalytic activities, which may be attributed to the decline in the light absorption of MAPbI<sub>3</sub> (Figure 5d).

Furthermore, the varies in catalytic activities of MAPbI<sub>3</sub> with reaction time are shown in Figure S16. As the reaction going on, the yield of butyl lactate increases almost linearly. The catalytic stability of MAPbI<sub>3</sub> is also investigated by recycling it in a refreshed reaction atmosphere every 2 h of continuous photocatalytic reaction (Figure S17). After cycling 3 times, the photocatalytic activities of MAPbI<sub>3</sub> decreases. The decreased intensity of diffraction peaks and the appearance of PbI<sub>2</sub> in XRD patterns indicates that the crystal structure of MAPbI<sub>3</sub> are partly destroyed after 3 cycles (Figure S18). Some protection strategies should be carried out to improve the photocatalytic stability of MAPbI<sub>3</sub> in the future. Additionally, Table S5 lists the catalytic performance comparison between MAPbI<sub>3</sub> and other homogeneous/heterogeneous catalysts. Compared with the condition with high temperature and high pressure, the visible light irradiation at ambient temperature used in this work generates a very competent performance.

## Conclusion

In conclusion, we employ the conversion of triose (DHA) as a probe reaction to investigate the surface termination in MAPbI<sub>3</sub> and further explore its role on the photocatalytic process. Specially, MAI-terminated MAPbI<sub>3</sub> exhibits good photocatalytic activities with the yield of 77 mg/L and the production rate of 7719 µg/g cat./h, respectively. By surface passivation experiment and ageing experiments, we further confirm that the exposed Pb(II) sites, caused by the oxidation of iodide on the MAI-terminated MAPbI<sub>3</sub> surface, play a crucial role in this photocatalytic synthesis reaction. Moreover, MAI-termination induces a p-type doping on MAPbI<sub>3</sub> surface, facilitating the photocatalytic synthesis of butyl lactate. The understanding on the surface regulation of MAPbI<sub>3</sub> may bring in new insights in the design of halide perovskite semiconductor materials for photocatalysis.

## Acknowledgements

This work was supported by the National Natural Science Foundation of China (21706080, 21975028, 51673025), China Postdoctoral Science Foundation (2019T120054, 2018M631359), National Key Research and Development Program of China Grant (2016YFB0700700), the start-up funding of BIT and Young Talent Thousand Program.

The authors also acknowledge Qin Du, Dr. Sai Ma, Dr. Lang Liu, Dr. Changli Chen, Dr. Yizhou Zhao, Dr. Na Liu, Dr. Xiuxiu Niu and Dr. Nengxu Li for helpful discussions.

**Keywords:** halide perovskite • surface termination • naked Pb(II) sites • photocatalysis • triose

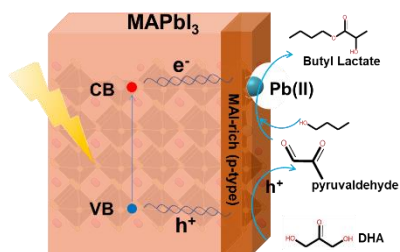
- [1] Best Research-Cell Efficiency Chart 2019, <https://www.nrel.gov/pv/cell-efficiency.html>.
- [2] J. Wang, J. Li, S. Lan, C. Fang, H. Shen, Q. Xiong, D. Li, *ACS Nano* **2019**, *13*, 5473-5484.
- [3] L. Zhao, K. M. Lee, K. Roh, S. U. Z. Khan, B. P. Rand, *Adv. Mater.* **2019**, *31*, 1805836.
- [4] N. Zhang, Y. Fan, K. Wang, Z. Gu, Y. Wang, L. Ge, S. Xiao, Q. Song, *Nat. Commun.* **2019**, *10*, 1770.
- [5] a) J. Peng, Y. Chen, K. Zheng, T. Pullerits, Z. Liang, *Chem. Soc. Rev.* **2017**, *46*, 5714-5729; b) Y. Dong, Y. Zhao, S. Zhang, Y. Dai, L. Liu, Y. Li, Q. Chen, *J. Mater. Chem. A* **2018**, *6*, 21729-21746.
- [6] a) Y.-F. Xu, M.-Z. Yang, B.-X. Chen, X.-D. Wang, H.-Y. Chen, D.-B. Kuang, C.-Y. Su, *J. Am. Chem. Soc.* **2017**, *139*, 5660-5663; b) K. Chen, X. Deng, G. Dodekatos, H. Tüysüz, *J. Am. Chem. Soc.* **2017**, *139*, 12267-12273; c) H. Huang, H. Yuan, K. P. F. Janssen, G. Solis-Fernández, Y. Wang, C. Y. X. Tan, D. Jonckheere, E. Debroye, J. Long, J. Hendrix, J. Hofkens, J. A. Steele, M. B. J. Roeffaers, *ACS Energy Lett.* **2018**, *3*, 755-759; d) Z. Zhang, Y. Liang, H. Huang, X. Liu, Q. Li, L. Chen, D. Xu, *Angew. Chem. Int. Ed.* **2019**, *58*, 7263-7267; e) X. Zhu, Y. Lin, Y. Sun, M. C. Beard, Y. Yan, *J. Am. Chem. Soc.* **2019**, *141*, 733-738; f) S. Park, W. J. Chang, C. W. Lee, S. Park, H.-Y. Ahn, K. T. Nam, *Nat. Energy* **2016**, *2*, 16185; g) Z. Hong, W. K. Chong, A. Y. R. Ng, M. Li, R. Ganguly, T. C. Sum, H. S. Soo, *Angewandte Chemie* **2019**, *58*, 3456-3460.
- [7] G. Gao, Q. Xi, H. Zhou, Y. Zhao, C. Wu, L. Wang, P. Guo, J. Xu, *Nanoscale* **2017**, *9*, 12032-12038.
- [8] S. Schünemann, M. van Gestel, H. Tüysüz, *ChemSusChem* **2018**, *11*, 2057-2061.
- [9] a) Y. Wu, P. Wang, X. Zhu, Q. Zhang, Z. Wang, Y. Liu, G. Zou, Y. Dai, M.-H. Whangbo, B. Huang, *Adv. Mater.* **2018**, *30*, 1704342; b) Y. Jiang, J.-F. Liao, Y.-F. Xu, H.-Y. Chen, X.-D. Wang, D.-B. Kuang, *J. Mater. Chem. A* **2019**, *7*, 13762-13769; c) Y. Jiang, J.-F. Liao, H.-Y. Chen, H.-H. Zhang, J.-Y. Li, X.-D. Wang, D.-B. Kuang, *Chem* **2020**; d) *Angew Chem Int Ed* **2018**; e) P. Qiu, Q. Wang, Y. Zhao, Y. Dai, Y. Dong, C. Chen, Q. Chen, Y. Li, *Frontiers in Chemistry* **2020**, *8*.
- [10] T. Hisatomi, J. Kubota, K. Domen, *Chem. Soc. Rev.* **2014**, *43*, 7520-7535.
- [11] Q. Wang, Y. Shao, H. Xie, L. Lyu, X. Liu, Y. Gao, J. Huang, *Appl. Phys. Lett.* **2014**, *105*, 163508.
- [12] E. Mosconi, J. M. Aspiroz, F. De Angelis, *Chem. Mater.* **2015**, *27*, 4885-4892.
- [13] a) C. Ran, J. Xu, W. Gao, C. Huang, S. Dou, *Chem. Soc. Rev.* **2018**, *47*, 4581-4610; b) Z. Liu, J. Hu, H. Jiao, L. Li, G. Zheng, Y. Chen, Y. Huang, Q. Zhang, C. Shen, Q. Chen, H. Zhou, *Adv. Mater.* **2017**, *29*, 1606774.
- [14] Y. Wang, W. Deng, B. Wang, Q. Zhang, X. Wan, Z. Tang, Y. Wang, C. Zhu, Z. Cao, G. Wang, H. Wan, *Nat. Commun.* **2013**, *4*, 2141.
- [15] H. Zhang, Z. Yang, W. Yu, H. Wang, W. Ma, X. Zong, C. Li, *Adv. Energy Mater.* **2018**, *8*, 1800795.
- [16] K. O. Brinkmann, J. Zhao, N. Pourdavoud, T. Becker, T. Hu, S. Olthof, K. Meerholz, L. Hoffmann, T. Gahlmann, R. Heiderhoff, M. F. Oszajca, N. A. Luechinger, D. Rogalla, Y. Chen, B. Cheng, T. Riedl, *Nature Communications* **2017**, *8*, 13938.
- [17] a) Y. Liu, K. Palotas, X. Yuan, T. Hou, H. Lin, Y. Li, S.-T. Lee, *ACS Nano* **2017**, *11*, 2060-2065; b) W.-J. Yin, T. Shi, Y. Yan, *Appl. Phys. Lett.* **2014**, *104*, 063903; c) A. Zohar, I. Levine, S. Gupta, O. Davidson, D. Azulay, O. Millo, I. Balberg, G. Hodes, D. Cahen, *ACS Energy Lett.* **2017**, *2*, 2408-2414.
- [18] a) L. Liu, S. Huang, Y. Lu, P. Liu, Y. Zhao, C. Shi, S. Zhang, J. Wu, H. Zhong, M. Sui, H. Zhou, H. Jin, Y. Li, Q. Chen, *Adv. Mater.* **2018**, *30*, 1800544; b) P. D. Akrivos, *Coordination Chemistry Reviews* **2001**, *213*, 181-210; c) J.-W. Lee, H.-S. Kim, N.-G. Park, *Accounts of Chemical Research* **2016**, *49*, 311-319.
- [19] a) H. Zhou, Q. Chen, G. Li, S. Luo, T.-b. Song, H.-S. Duan, Z. Hong, J. You, Y. Liu, Y. Yang, *Science* **2014**, *345*, 542-546; b) J. You, Y. Yang, Z. Hong, T.-B. Song, L. Meng, Y. Liu, C. Jiang, H. Zhou, W.-H. Chang, G. Li, Y. Yang, *Appl. Phys. Lett.* **2014**, *105*, 183902.
- [20] a) Q.-Q. Ge, J. Ding, J. Liu, J.-Y. Ma, Y.-X. Chen, X.-X. Gao, L.-J. Wang, J.-S. Hu, *J. Mater. Chem. A* **2016**, *4*, 13458-13467; b) S. R. Raga, M.-C. Jung, M. V. Lee, M. R. Leyden, Y. Kato, Y. Qi, *Chem. Mater.* **2015**, *27*, 1597-1603.
- [21] G. E. Eperon, S. N. Habisreutinger, T. Leijtens, B. J. Bruijns, J. J. van Franeker, D. W. deQuilettes, S. Pathak, R. J. Sutton, G. Grancini, D. S. Ginger, R. A. J. Janssen, A. Petrozza, H. J. Snaith, *ACS Nano* **2015**, *9*, 9380-9393.
- [22] a) S. Berweger, G. A. MacDonald, M. Yang, K. J. Coakley, J. J. Berry, K. Zhu, F. W. DelRio, T. M. Wallis, P. Kabos, *Nano Letters* **2017**, *17*, 1796-1801; b) J. Huang, S. Tan, P. D. Lund, H. Zhou, *Energy & Environmental Science* **2017**, *10*, 2284-2311.
- [23] Y. Chen, N. Li, L. Wang, L. Li, Z. Xu, H. Jiao, P. Liu, C. Zhu, H. Zai, M. Sun, W. Zou, S. Zhang, G. Xing, X. Liu, J. Wang, D. Li, B. Huang, Q. Chen, H. Zhou, *Nat. Commun.* **2019**, *10*, 1112.
- [24] G. Grancini, V. D'Innocenzo, E. R. Dohner, N. Martino, A. R. Srimath Kandada, E. Mosconi, F. De Angelis, H. I. Karunadasa, E. T. Hoke, A. Petrozza, *Chem. Sci.* **2015**, *6*, 7305-7310.

## RESEARCH ARTICLE

- [25] Y. T. Prabhu, K. V. Rao, V. S. S. Kumar, B. S. Kumari, *World Journal of Nano Science and Engineering* **2014**, *4*, 21-28.
- [26] a) V. M. Pereira, A. H. Castro Neto, *Phys. Rev. Lett.* **2009**, *103*, 046801; b) S.-M. Choi, S.-H. Jhi, Y.-W. Son, *Phys. Rev. B* **2010**, *81*, 081407; c) L. Wang, Z. Zeng, W. Gao, T. Maxson, D. Raciti, M. Giroux, X. Pan, C. Wang, J. Greeley, *Science* **2019**, *363*, 870-874.
- [27] a) Y. Li, X. Xu, C. Wang, C. Wang, F. Xie, J. Yang, Y. Gao, *J. Phys. Chem. C* **2015**, *119*, 23996-24002; b) Y. Wang, W.-Y. Rho, H.-Y. Yang, T. Mahmoudi, S. Seo, D.-H. Lee, Y.-B. Hahn, *Nano Energy* **2016**, *27*, 535-544.
- [28] Y. Hayashi, Y. Sasaki, *Chem. Commun.* **2005**, 2716-2718.
- [29] M. S. Holm, S. Saravanamurugan, E. Taarning, *Science* **2010**, *328*, 602-605.
- [30] a) M. Bellardita, A. Di Paola, B. Megna, L. Palmisano, *Appl. Catal. B-Environ.* **2017**, *201*, 150-158; b) M. Toyoda, Y. Nanbu, Y. Nakazawa, M. Hirano, M. Inagaki, *Appl. Catal. B-Environ.* **2004**, *49*, 227-232.
- [31] B. Murali, S. Dey, A. L. Abdelhady, W. Peng, E. Alarousu, A. R. Kirmani, N. Cho, S. P. Sarmah, M. R. Parida, M. I. Saidaminov, A. A. Zhumekenov, J. Sun, M. S. Alias, E. Yengel, B. S. Ooi, A. Amassian, O. M. Bakr, O. F. Mohammed, *ACS Energy Lett.* **2016**, *1*, 1119-1126.
- [32] A. Mehta, J. Im, B. H. Kim, H. Min, R. Nie, S. I. Seok, *ACS nano* **2018**, *12*, 12129-12139.

## RESEARCH ARTICLE

## Entry for the Table of Contents



MAI-terminated MAPbI<sub>3</sub> could convert DHA into butyl lactate with the production rate of 7719 μg/g cat./h under visible light illumination. Specially, MAI-termination induces p-doping effect near the surface, leading to the oxidation of DHA into pyruvaldehyde. Moreover, MAI-termination is susceptible to iodide oxidation, resulting in the Pb(II) sites exposed, which further promote the reaction of pyruvaldehyde and butanol to produce butyl lactate.

Institute and/or researcher Twitter usernames: ((optional))